



HAL
open science

Multiscale time-resolved fluorescence study of a glycogen phosphorylase inhibitor combined with quantum chemistry calculations

Valentin Maffeis, Konstantinos Mavreas, Filippo Monti, Michael Mamais, Thomas Gustavsson, Evangelia Chrysina, Dimitra Markovitsi, Thanasis Gimisis, Alessandro Venturini

► To cite this version:

Valentin Maffeis, Konstantinos Mavreas, Filippo Monti, Michael Mamais, Thomas Gustavsson, et al.. Multiscale time-resolved fluorescence study of a glycogen phosphorylase inhibitor combined with quantum chemistry calculations. *Physical Chemistry Chemical Physics*, 2019, 21 (14), pp.7685-7696. 10.1039/C8CP07538G . cea-02096313

HAL Id: cea-02096313

<https://cea.hal.science/cea-02096313>

Submitted on 23 Oct 2019

HAL is a multi-disciplinary open access archive for the deposit and dissemination of scientific research documents, whether they are published or not. The documents may come from teaching and research institutions in France or abroad, or from public or private research centers.

L'archive ouverte pluridisciplinaire **HAL**, est destinée au dépôt et à la diffusion de documents scientifiques de niveau recherche, publiés ou non, émanant des établissements d'enseignement et de recherche français ou étrangers, des laboratoires publics ou privés.



Cite this: *Phys. Chem. Chem. Phys.*,
2019, 21, 7685

Multiscale time-resolved fluorescence study of a glycogen phosphorylase inhibitor combined with quantum chemistry calculations†

Valentin Maffei,^{‡a} Konstantinos Mavreas,^{‡b} Filippo Monti,^{‡c}
Michael Mamais,^{‡abd} Thomas Gustavsson,^{‡a} Evangelia D. Chrysina,^d
Dimitra Markovitsi,^{‡*a} Thanasis Gimisis^{‡*b} and Alessandro Venturini^{*c}

A fluorescence study of N^1 -(β -D-glucopyranosyl)- N^4 -[2-acridin-9(10H)-onyl]-cytosine (GLAC), the first fluorescent potent inhibitor of glycogen phosphorylase (GP), in neutral aqueous solution, is presented herein. Quantum chemistry (TD-DFT) calculations show the existence of several conformers both in the ground and first excited states. They result from rotations of the acridone and cytosine moieties around an NH bridge which may lead to the formation of non-emitting charge-transfer states. The fingerprints of various conformers have been detected by time-resolved fluorescence spectroscopy (fluorescence upconversion and time-correlated single photon counting) and identified using as criteria their energy, polarization and relative population resulting from computations. Such an analysis should contribute to the design of new GP inhibitors with better fluorescence properties, suitable for imaging applications.

Received 10th December 2018,
Accepted 1st March 2019

DOI: 10.1039/c8cp07538g

rsc.li/pccp

1 Introduction

Glycogen phosphorylase (GP), a highly regulated enzyme involved in glycogenolysis, has been used, in recent years, as a molecular target for the development of new antidiabetics.^{1–6} Recently, we reported the synthesis and crystallographic study of a glucose-based acridone derivative, N^1 -(β -D-glucopyranosyl)- N^4 -[2-acridin-9(10H)-onyl]-cytosine (GLAC), which was found to be among the most potent rabbit muscle GP inhibitors.⁴ In addition to its promising therapeutic action, GLAC was shown to be also an interesting optical probe for sensing the enzyme catalytic site. As the lowest in energy electronic absorption band of GLAC is well-separated from those of GP, it provides information about its interaction with the enzyme. Thus, it was shown that, upon binding to GP, GLAC experiences a significantly more basic environment compared to that of the bulk aqueous solvent.⁴

Here, we show that GLAC emits fluorescence both when it is free in neutral aqueous solution and when it is bound to the enzyme. In recent years, the intrinsic fluorescence of inhibitors has been used for the study of their binding to various types of enzymes (see, for example, ref. 7–11). Fluorescence offers another route for sensing the local environment, not only in a static mode, where all effects are averaged, but also in a dynamic way thanks to time-resolved spectroscopy.^{12–14} This has, in particular, been successfully applied to study drug–protein complexes (see, for example, ref. 15–17). To our knowledge, none of the previously reported catalytic site inhibitors of GP provides this possibility.

The most important part of the present work concerns free GLAC in aqueous neutral solution, where it is present in its anionic form,⁴ noted GLAC^{-1} (Fig. 1). It is performed by combining steady-state and time-resolved fluorescence spectroscopies. For the latter, two different detection techniques were used, namely fluorescence upconversion (FU) and time-correlated single photon counting (TCSPC), with the same laser source providing 120 fs pulses at 400 nm. This approach allows us to

^a LIDYL, CEA, CNRS, Université Paris-Saclay, Gif-sur-Yvette, France.
E-mail: dimitra.markovitsi@cea.fr

^b Department of Chemistry, National and Kapodistrian University of Athens, Athens, Greece. E-mail: gimisis@chem.uoa.gr

^c Istituto ISOF, Consiglio Nazionale delle Ricerche, Bologna, Italy.
E-mail: alessandro.venturini@isof.cnr.it

^d Institute of Biology, Medicinal Chemistry & Biotechnology, National Hellenic Research Foundation, Athens, Greece. E-mail: echrysina@eie.gr

† Electronic supplementary information (ESI) available: Synthetic, spectroscopic and theoretical calculation details. See DOI: 10.1039/c8cp07538g

‡ These authors contributed equally.

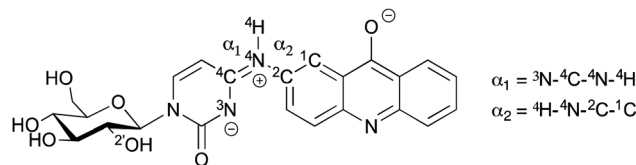


Fig. 1 Schematic representation of GLAC^{-1} in neutral aqueous solution (α_1 and α_2 designate dihedral angles).

explore fluorescence decays and fluorescence anisotropies from the femtosecond to the nanosecond time-scales. A few comparative experiments were also performed for acetonitrile solutions, where the neutral form of GLAC is present.

The experimental results are interpreted with the help of quantum-mechanical calculations based on the time-dependent density functional theory (TD-DFT), including implicit solvent *via* the polarizable continuum model (PCM).

A detailed study of the free GLAC fluorescence is necessary before tackling its behaviour when it is bound to the enzyme. As a matter of fact, its emission properties are strongly affected by conformational factors, related to multiple rotations around the dihedral angles α_1 and α_2 (Fig. 1), which give rise to complex potential energy surfaces (PES). Their disentanglement in this first step of the study, will allow us to assess, in a second step, additional factors that intervene in the GLAC/GP complex.

2 Methodological details

2.1 Synthesis

2-((4-Acetamidophenyl)amino)benzoic acid. To a solution of 2-aminobenzoic acid (2.77 g, 18.6 mmol) and 4-aminoacetanilide (2.79 g, 17.7 mmol) in 7 ml of diethylene glycol was gradually added, under stirring, anhydrous potassium carbonate (2.44 g, 17.5 mmol). After cessation of gas evolution, to the mixture were added freshly precipitated copper powder¹⁸ (100 mg, 1.57 mmol) and copper(i) oxide (100 mg, 0.70 mmol) and the whole mixture was heated under argon at 150 °C for 8 h. The mixture was cooled to room temperature and filtered. A small portion of sodium metabisulfite was added to the filtrate, which then was acidified with 30 ml of 1 N HCl. The precipitated solid was filtered, washed with water and dried to yield 2.77 g (58%) of the title compound, as a grayish powder. ¹H NMR (200 MHz, DMSO-*d*₆) δ 9.94 (s, 1H), 9.53 (s, 1H), 7.87 (dd, *J* = 7.9, 1.6 Hz, 1H), 7.57 (d, *J* = 8.7 Hz, 2H), 7.35 (ddd, *J* = 8.6, 7.1, 1.7 Hz, 1H), 7.17 (d, *J* = 8.7 Hz, 2H), 7.08 (d, *J* = 8.4 Hz, 1H), 6.72 (t, *J* = 7.5 Hz, 1H), 2.03 (s, 3H).

4-Aminoacridone. 2-((4-Acetamidophenyl)amino)benzoic acid (920 mg, 3.40 mmol) was cyclised and deacetylated by the procedure described in the literature.¹⁹ The solid which precipitated during neutralisation was filtered, washed with copious amounts of water and dried under vacuum to afford the title compound (580 mg, 81%) as a greenish-yellow powder. The analytical data were in accordance with those previously reported.⁴

GLAC was prepared following our previously published protocol.^{4,20}

2.2 Spectroscopic measurements

For the majority of the experiments, a stock solution of GLAC in dimethyl sulfoxide (DMSO, UVASOL Merck, 2.4 mM) was prepared and aliquots of the stock solution were diluted with ultrapure water (Milli-Q Synthesis) either in a phosphate buffer (0.015 mol L⁻¹ NaH₂PO₄, 0.015 mol L⁻¹ Na₂HPO₄; pH 7; ingredients from Fluka), or in acetonitrile (UVASOL Merck). For the alkaline solution (pH = 12.7), 0.113 mol L⁻¹

NaOH/0.087 mol L⁻¹ KCl (Fluka) were used. The final concentration of DMSO was ~1% v/v, in all solutions.

For steady-state and TCSPC measurements, GLAC was studied both in water and in buffer (pH = 7.00), inside 1 cm × 1 cm quartz cells, and no difference was detected (Fig. S1, ESI†). For FU measurements, only water solutions were studied. In the latter case, a rotating QZ cell with an optical path of 1 mm was used. For all fluorescence measurements, the signal obtained for the neat solvent was negligible compared to the GLAC signal.

Absorption was recorded using a PerkinElmer Lambda 900 instrument. Two different instruments were used for fluorescence spectra: a Shimadzu RF 5310 PC and a SPEX Fluorolog-3 fluorimeter equipped with a double monochromator on the emission side, the spectra obtained with the latter apparatus were corrected for the spectral response of the detection system. For the determination of fluorescence quantum yields (ϕ) the absorbance at the excitation wavelength was on the order of 0.01.

The excitation source for time-resolved experiments was the second harmonic (400 nm, 120 fs) of a Ti-sapphire laser (Coherent MIRA 900). The repetition rate was 76 MHz for FU but reduced to 4.75 MHz for TCSPC using a pulse picker (Coherent 9200). The homebuilt FU setup is described in detail elsewhere.²¹ The sample fluorescence was collected with two parabolic mirrors and mixed with the residual 800 nm fundamental beam in a 0.5 mm type I BBO crystal. The up-converted signal was spectrally filtered by a double-grating monochromator (SPEX 1680, spectral resolution *ca.* 5 nm) and detected by a photomultiplier (Hamamatsu 1527P) coupled to a photon counter (Stanford SR400). The apparatus function was *ca.* 330 fs (fwhm). The TCSPC setup uses a Becker & Hickl GmbH SPC630 card controlled by a home-made LabView program. The fluorescence was spectrally resolved by a small monochromator (HR250, Jobin-Yvon) and then detected by a microchannel plate (R1564 U Hamamatsu). Part of the IR laser pulse was detected by a fast photodiode (ThorLabs) for the synchronisation. The instrumental response function was about 60 ps (fwhm), as determined by the Raman line corresponding to the O–H stretching of the water molecule.

In both time-resolved experiments (TCSPC and FU), only the vertically polarised fluorescence was detected. Consequently, the parallel (I_{par}) and perpendicular (I_{perp}) components of the total fluorescence signals were recorded by varying the polarization, vertical or horizontal, of the exciting beam with a zero-order half-wave plate (in the FU setup) or with a Fresnel rhomb (in the TCSPC setup). As the excitation energies measured after the half-wave plate were identical under parallel and perpendicular conditions, the *G* factor was set equal to 1 (*i.e.* no corrections were made). The total fluorescence kinetics $F(t)$ and the fluorescence anisotropies $r(t)$ were constructed according to the equations:

$$F(t) = I_{\text{par}}(t) + 2GI_{\text{perp}}(t)$$

and

$$r(t) = (I_{\text{par}}(t) - GI_{\text{perp}}(t))/(I_{\text{par}}(t) + 2GI_{\text{perp}}(t)).$$

2.3 Theoretical part

The calculations were performed with DFT and its time dependent extension TD-DFT²² with implicit water (PCM)²³ as implemented in Gaussian 16.²⁴ The density functional utilised for the optimisation of the conformers in the ground state and in the first excited state was M062X²⁵ at the 6-311g** basis set level. The calculations include the solvent effects (PCM) in the LR (linear response) formalism in the case of absorption.^{26,27} On the other hand, emission has been calculated using the SS (State-Specific) model which is more appropriate for dark states with an oscillator strength of almost zero. This procedure uses the SCRF facility “external-iteration” to carry out a non-equilibrium solvation calculation. It involves the relaxation of the ground state density due to the solvent with respect to the specific excitation under investigation.^{28,29}

Absorption and emission spectra were calculated at the PCM/M062X/6-311+g**//PCM/M062X/6-311g** level. For optimization and single point calculations of the S_1 excited state, the six energetically lowest excited singlet states were used. The stationary points in the ground and excited states were characterized by frequency calculation. Thermochemical analysis (free energy, ΔG) was performed at 298.15 K, starting from the frequency calculations.

The charge transfer character of our systems has been evaluated using Ciofini's D_{CT} charge transfer indexes³⁰ in the framework of the Gaussian 16 software package. The index (D_{CT}) gives a measure of the nature of the electronic reorganization occurring upon an electronic excitation.

3 Experimental results

The lowest-energy absorption band of GLAC in neutral aqueous solution is characterised by a peak at 405 nm and a shoulder at around 391 nm. The maximum molar absorption coefficient is $5300 \pm 100 \text{ mol}^{-1} \text{ L cm}^{-1}$. Excitation at this band gives rise to two poorly resolved broad fluorescent peaks of almost equal intensity, centred at 455 and $474 \pm 2 \text{ nm}$ (63 and 60 kcal mol^{-1} , respectively). Varying the excitation wavelength between 315 nm ($90.8 \text{ kcal mol}^{-1}$) and 435 nm ($65.7 \text{ kcal mol}^{-1}$) does not induce any change either in the shape or in the intensity of the spectrum, corrected for the absorbed photons (Fig. S2a, ESI[†]). In Fig. 2a are shown the absorption and fluorescence spectra on an energy scale; for the conversion, the emission intensity at wavelength λ has been multiplied by λ^2 .

The fluorescence quantum yield ϕ , determined for GLAC in the 5–8 pH range, with excitation at 410 nm, using Coumarin 153 in cyclohexane as a reference ($\phi = 0.90$),³¹ is 0.09 ± 0.01 . In strongly basic solutions (> 12.7), where GLAC exists as a bis-anion,⁴ fluorescence vanishes nearly completely, its intensity being lower than 2% compared to that observed for neutral solutions (Fig. 2a). When GLAC is bound to the enzyme, the intensity of the fluorescence spectrum decreases to about one tenth and its shape changes slightly. We still observe two poorly resolved peaks, but, in contrast to free GLAC, the peak at shorter wavelength is more intense.

Time-resolved fluorescence signals were recorded at 430, 465 and 515 nm (illustrated in Fig. 2b) over three different time scales: 9 ps, 100 ps and 40 ns.

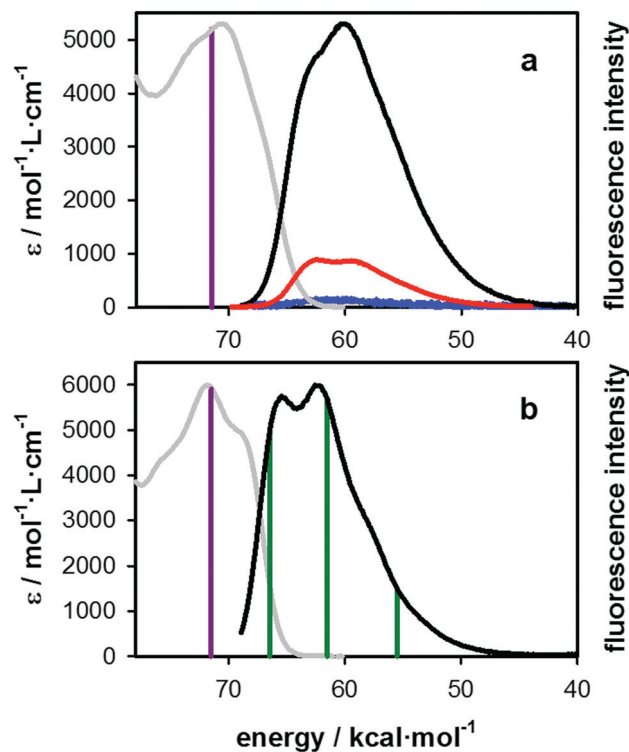


Fig. 2 Steady-state absorption (grey) and corrected fluorescence spectra of GLAC in (a) buffered aqueous solution (pH 7) and (b) acetonitrile. The vertical violet lines indicate the excitation wavelength (400 nm) used in the time-resolved experiments. The red and blue spectra in (a) have been obtained, respectively, for GLAC in pH 12.7 and the GP:GLAC complex in the assay used in ref. 4 (molar ratios 1.0:0.9). Fluorescence intensities in (a) are representative of the quantum yields. Green vertical lines in (b) correspond to the wavelengths at which time-resolved signals have been recorded. Excitation wavelength: 410 nm.

The total fluorescence intensity exhibits a complex pattern, in particular at early times (Fig. 3a). Within the first 10 ps, the signal on the blue side of the emission spectrum loses about 60% of its amplitude. The opposite behaviour is detected on the red side, where a 10% rise is observed on the same time-scale. After 20 ps, the fluorescence detected at all the probed wavelengths decreases monotonically. On the ns time-scale, the decay at 430 nm is significantly faster compared to those at 465 and 515 nm, which are rather similar (Fig. 3b). At 40 ns, the signal amplitude is lower than its initial value by more than two orders of magnitude (Fig. S1, ESI[†]).

In order to obtain a quantitative description of the fluorescence kinetics, first, the $F(t)$ signals obtained by TCSPC were fitted using tri-exponential model functions, $f(t) = a_1 \exp(-t/\tau_1) + a_2 \exp(-t/\tau_2) + a_0 \exp(-t/\tau_0)$, convoluted by the apparatus function. The parameters derived from the fits are given in Table 1. The values found for the time constant τ_0 are well below the time-resolution of the experiment and their weight, $w_0 = a_0 \tau_0 / \sum a_i \tau_i$, to the TCSPC signals, is negligible (< 0.01). As this ultrafast component is resolved by FU, its features are not included in Table 1. The time constants τ_1 and τ_2 were found to be the same at all three probed wavelengths, $7.9 \pm 0.1 \text{ ns}$ and

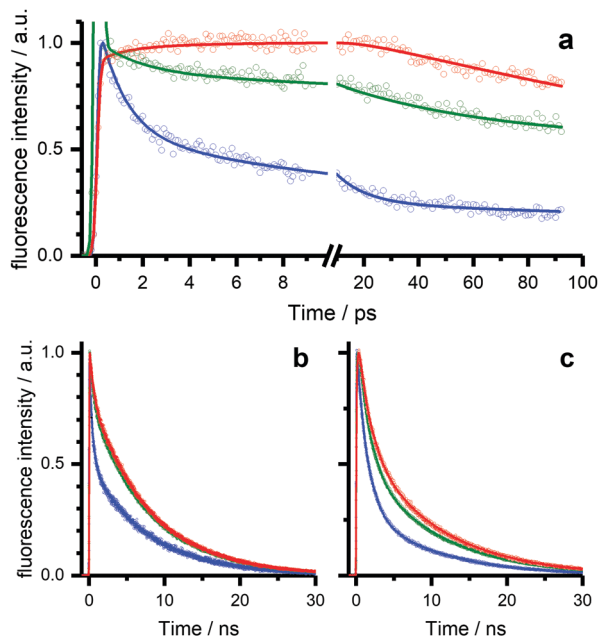


Fig. 3 Total fluorescence of GLAC in neutral aqueous solution (a) and (b) and acetonitrile (c) at 430 (blue), 465 (green) and 515 nm (red) by fluorescence upconversion (a) and time-correlated single photon counting (b) and (c); circles and solid lines correspond, respectively, to experimental points and fitted functions (see Table 1); excitation wavelength: 400 nm. The green spark in (a) is due to the Raman emission of water.

0.5 ± 0.1 ns, respectively, but the corresponding amplitudes are strongly wavelength dependent. It is clear that the fluorescence spectrum is dominated by the longest component, because at its most intense part w_1 amounts to 0.97. Even if the amplitude of the shorter component at 430 nm is 0.5, its contribution to the total fluorescence at this wavelength is only 6% and smaller at longer wavelengths.

The $F(t)$ signals obtained by FU were fitted by four-exponential model function; $f(t) = a_1 \exp(-t/\tau_1) + a_2 \exp(-t/\tau_2) + a_3 \exp(-t/\tau_3) + a_4 \exp(-t/\tau_4)$, where the two time constants τ_1 and τ_2 were fixed to the values derived from the TCSPC measurements (Table 1) while τ_3 and τ_4 were free-floating. The absolute values of the time constants τ_3 (~ 11 ps) and τ_4 (~ 1 ps) are similar for all the probed wavelengths but have opposite signs in the red and the blue part of the spectrum.

The fluorescence anisotropy traces are presented in Fig. 4. All of them decay monotonously, reaching zero in about 1.5 ns.

The initial r_0 values decrease with increasing emission wavelength. Combined fits of the $r(t)$ signals determined by FU and TCSPC at a given emission wavelength with bi-exponential model functions, $a_{r1} \exp(-t/\tau_{r1}) + a_{r2} \exp(-t/\tau_{r2})$, were performed.

The resulting fitted parameters are gathered in Table 2, where the values of the time-zero anisotropy r_0 as well the average depolarization time $\langle \tau_r \rangle = (a_{r1}\tau_{r1} + a_{r2}\tau_{r2})/(a_{r1} + a_{r2})$ are also shown. The two time constants derived from the fits are similar at the three probed wavelengths: $\tau_{r1} = 280 \pm 10$ ps and $\tau_{r2} = 20 \pm 1$ ps. When going from the blue to the red side of the spectrum, the average depolarization time, determined as $\langle \tau_r \rangle = (a_{r1}\tau_{r1} + a_{r2}\tau_{r2})/(a_{r1} + a_{r2})$, increases from 121 to 188 ps.

Going from neutral aqueous solutions to acetonitrile, both the absorption and the fluorescence spectra shift to higher energies (Fig. 2b), while the fluorescence quantum yield increases from 0.09 to 0.22. The fluorescence spectra, still independent of the excitation wavelength (Fig. S2b, ESI[†]), exhibit now two clearly distinguishable peaks. The fluorescence decays recorded by TCSPC (Fig. 3c) can be fitted by a bi-exponential model function providing two nanosecond components: $\tau_1 = 9.7 \pm 1$ ns and $\tau_2 = 1.3 \pm 1$ ns (Table 1). Both of them are longer than their counterpart in phosphate buffer. This is particularly true for τ_2 , predominant at the blue part of the spectrum, whose weight increases significantly. Thus, we can reasonably correlate τ_2 with the higher energy peak.

4 Theoretical results

In order to get a deeper insight into the spectroscopic findings reported above, DFT and TD-DFT calculations have been carried out to map the potential energy surface (PES) of the anionic form of GLAC, both in the ground state (S_0) and in its lowest electronic excited state (S_1).

4.1 Ground state

In the ground-state, our calculations, identified for GLAC^{-1} four classes of stable conformers (labelled **A**, **B**, **C** and **D**) that, for steric hindrance reasons, correspond to seven thermally-accessible minima labelled as **GS-X**, where **X** = **A'**, **A''**, **B**, **C'**, **C''**, **D'** and **D''**. Moreover, nine transition states were found on S_0 ; they are labelled as **TS GS-XY**, where **X** and **Y** are different minima (e.g., **TS GS-AB** indicates the transition state between **GS-A** and **GS-B**).

Table 1 Parameters derived from the fits of total fluorescence signals $F(t)$ obtained by TCSPC and FU with multi-exponential functions $\sum a_i \exp(-t/\tau_i)$; $w_i = a_i \tau_i / (\sum a_i \tau_i)$ represents the weight of component i to the $F(t)$ determined by each technique

λ (nm)	TCSPC		FU	
	τ_1 (ns) (a_1, w_1)	τ_2 (ns) (a_2, w_2)	τ_3 (ps) (a_3)	τ_4 (ps) (a_4)
430 ^a	7.9 ± 0.1 (0.50, 0.94)	0.5 ± 0.1 (0.50, 0.06)	11.4 ± 0.4 (0.30)	1.1 ± 0.1 (0.47)
465 ^a	7.7 ± 0.1 (0.69, 0.97)	0.5 ± 0.1 (0.31, 0.03)	11.9 ± 0.5 (0.21)	0.6 ± 0.4 (0.05) ^c
515 ^a	7.9 ± 0.1 (0.73, 0.97)	0.6 ± 0.1 (0.27, 0.03)	-11.5 ± 1.5 (0.11)	-1.1 ± 0.1 (0.07)
430 ^b	9.6 ± 0.1 (0.28, 0.74)	1.3 ± 0.1 (0.72, 0.26)	—	—
465 ^b	9.7 ± 0.1 (0.44, 0.85)	1.3 ± 0.1 (0.56, 0.15)	—	—
515 ^b	9.6 ± 0.1 (0.51, 0.88)	1.4 ± 0.1 (0.49, 0.12)	—	—

^a In PBS buffer (pH = 7). ^b In acetonitrile. ^c Large errors due to superposition of the Raman line of water.

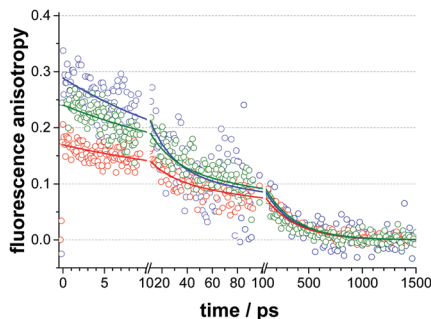


Fig. 4 Fluorescence anisotropy determined for GLAC at 430 (blue), 565 (green) and 515 nm (red) by fluorescence upconversion and time-correlated single photon counting; circles and solid lines correspond, respectively, to experimental points and fitted functions (Table 2); excitation wavelength: 400 nm.

Table 2 Parameters derived from combined fits of fluorescence anisotropy $r(t)$ obtained by TCSPC and FU at the same wavelength with bi-exponential functions $a_{r1} \exp(-t/\tau_{r1}) + a_{r2} \exp(-t/\tau_{r2})$. Time constants in ps; $\langle \tau_r \rangle = (a_{r1}\tau_{r1} + a_{r2}\tau_{r2})/(a_{r1} + a_{r2})$ represents the average depolarization time and r_0 the time-zero anisotropy

λ (nm)	τ_{r1} (a_{r1})	τ_{r2} (a_{r2})	r_0	$\langle \tau_r \rangle$
430	270 ± 10 (0.12)	$19 \pm (0.16)$	0.28	127 ± 21
465	280 ± 10 (0.13)	$20 \pm (0.11)$	0.24	161 ± 20
515	290 ± 10 (0.11)	$21 \pm (0.06)$	0.17	188 ± 15

The particularly high number of detected conformers is due to all the possible rotations around the two dihedral angles formed by the NH bridge linking the two planar acridone and cytosine moieties (*i.e.*, α_1 and α_2 in Fig. 1). The energy difference between all the conformers is always within $1.5 \text{ kcal mol}^{-1}$, so they are all populated at room temperature. It is worth noting that, in all conformers, the glucose substituent is almost perpendicular to the plane of the cytosine group, to which it is linked, forming a hydrogen bond between the 2'-OH group of the sugar and the carbonyl oxygen in the cytosine ring.

The asymmetry of the glucose moiety prevents GLAC⁻¹ from having a symmetry plane (*i.e.*, the plane of the paper in Fig. 1) even in completely planar conformers (*i.e.*, GS-B). In other cases, for steric hindrance reasons, the molecule is unable to reach complete planarity and couples of almost mirrored minima are found (*e.g.*, GS-A' and GS-A''). In Table S1 (ESI[†]) are summarized the data corresponding to all conformers. It can be seen that these pairs of mirrored minima have almost the same geometrical characteristics, energies and spectroscopic properties. In Fig. 5 are depicted all seven ground-state conformers of GLAC⁻¹, grouped as pairs of minima for non-planar structures (*i.e.*, GS-A' and GS-A'', GS-C' and GS-C'', GS-D' and GS-D''). We also grouped them as geometric *Z-E* isomers, depending on the orientation around the ⁴C-⁴N bond (α_1 dihedral), which, in all cases, has a double bond character (see Fig. 1). Ground-state conformers A'-A'' and B are geometric *Z* isomers, while C'-C'' and D'-D'' are *E* isomers.

The rotation around α_1 requires the system to overcome high energy barriers (*e.g.*, the TS GS-A''C'' or TS GS-BD'') are located

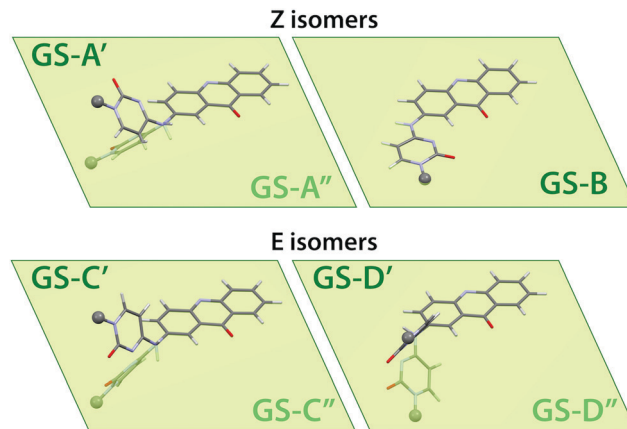


Fig. 5 Ground-state conformer pairs, reflected on a common "acridone plane". The spheres represent the glucose moiety. In all minima, the NH bridge is virtually coplanar with the cytosine moiety.

around 13 kcal mol^{-1} above the corresponding minima). This is due to the higher double-bond character of the ⁴C-⁴N bond, compared to the ⁴N-²C bond. This evidence is corroborated by the shorter average length of the ⁴C-⁴N bond with respect to the ⁴N-²C one (*i.e.*, 1.35 \AA vs. 1.42 \AA , for all the conformers, see Table S2, ESI[†]).

In Fig. 6, the bi-dimensional S₀ PES (potential-energy surface) of GLAC⁻¹ is reported as a function of α_1 and α_2 . According to what was stated above, all minima display only two ranges of α_1 values (indicated with green bands in Fig. 6): one is close

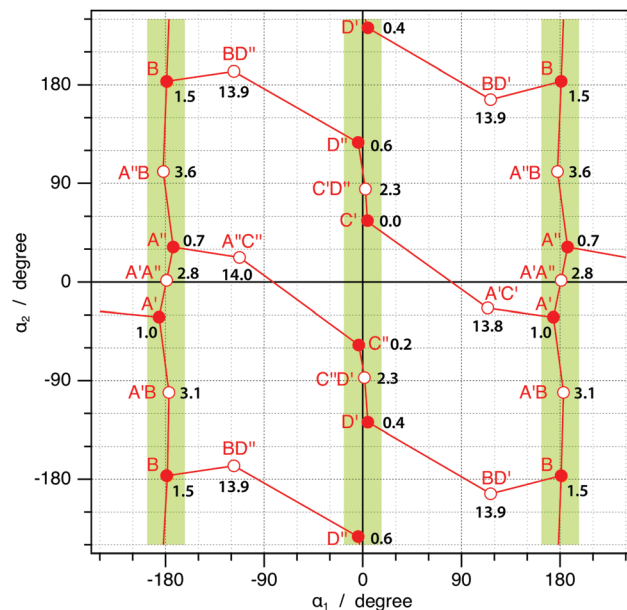


Fig. 6 Bi-dimensional conformational PES of GLAC⁻¹ in the ground state. The numbers indicated are the $\Delta\Delta G$ energies in kcal mol^{-1} relative to the more stable minimum C'. Filled circles are minima and empty circles are transition states. Red lines indicate the real connections between conformers. Also highlighted with a green band, are the zones where α_1 is almost 0° or $\pm 180^\circ$. In all GS minima, the NH bridge is virtually coplanar with the cytosine moiety. Notation: A' corresponds to the minimum GS-A' and A'B to the TS GS-A'B.

to 0° , corresponding to *E* conformers (*i.e.*, **GS-C'**, **GS-C''**, **GS-D'** and **GS-D''**); the other is close to 180° , corresponding to *Z* conformers (*i.e.*, **GS-A'**, **GS-A''** and **GS-B**).

On the contrary, the α_2 values associated with minima are more spread out and the energy barriers due to the rotation around α_2 (in which the NH bridge remains coplanar with the cytosine moiety) are always smaller than $4.0 \text{ kcal mol}^{-1}$ (see Fig. 6); this is a strong indication of the single character of the ${}^4\text{N}-{}^2\text{C}$ bond. It should be emphasised that the previously mentioned mirrored couples of conformers simply differ by an opposite rotation around α_2 (*e.g.*, $\alpha_2 = 0^\circ \pm 32^\circ$ in **GS-A''** and **GS-A'**, respectively, compare Fig. 5 and 6).

Another important point to stress is that, despite all conformers being virtually reachable from any point of the S_0 PES, it is impossible to directly go from **GS-C'** to **GS-C''** and from **GS-D'** to **GS-D''**. In fact, the two planar transition states **TS GS-C'C''** ($\alpha_1 = \alpha_2 = 0^\circ$) and **TS GS-C'C''** ($\alpha_1 = 0^\circ$ and $\alpha_2 = 180^\circ$) were not found, due to the steric hindrance between the hydrogen atoms of the acridone and cytosine moieties.

4.2 Excited state

In order to rationalize the excited-state processes experimentally observed in GLAC^{-1} , we investigated the PES of its lowest excited state (*i.e.*, S_1), starting from the geometries of all seven minima previously found in the ground state. In Fig. 7, the S_1 PES is depicted as a function of both α_1 and α_2 dihedral angles. Upon relaxation from the Frank-Condon regions, we were able to locate ten minima on the S_1 PES (see Table S3, ESI†).

Upon $S_0 \rightarrow S_1$ excitation, both **GS-A'** and **GS-A''** conformers relax to the same excited-state minimum (*i.e.*, **ES-A**), which is planar, like the one directly reached from **GS-B** (*i.e.*, **ES-B**). These two planar excited-state conformers display the same α_1 dihedral angle (*i.e.*, $\alpha_1 = 180^\circ$), but different values of α_2 (*i.e.*, $\alpha_2 = 0^\circ$ or 180° for **ES-A** and **ES-B**, respectively).

On the other hand, the excited-state planarization of α_2 is not observed upon relaxation of the remaining conformers (*i.e.*, **C'**, **C''**, **D'** and **D''**); accordingly, four corresponding minima are also found on the S_1 potential-energy surface.

It is worth noting that two extra couples of minima (*i.e.*, **ES-E'** and **ES-E''**, **ES-F'** and **ES-F''**), which do not have their counterparts on S_0 , were found on the S_1 PES. All the geometries of these new excited-state minima display α_1 angles around $\pm 90^\circ$ (yellow bands in Fig. 7), meaning that the two aromatic moieties of GLAC^{-1} turn out to be mutually orthogonal (Fig. 8), leading to the formation of a twisted intramolecular charge-transfer (TICT) state. These four twisted minima display $\alpha_2 \approx 0^\circ$ or 180° , meaning that the lone pair of the NH bridge always overlaps with the π orbitals of the acridone moiety (see Fig. 8).

Analysis of the S_1 PES and of other six states included in the calculation shows that the formation of the four charge-transfer dark states (TICT) does not correspond to crossing of different states but is simply due to a charge-shift between the acridone and cytosine moieties in S_1 . This charge-shift is also indicated by the calculated D_{CT} indexes. They show the difference of the non-emitting states with the other S_1 minima (see Table S4 for the values and Fig. S3, ESI† for a graphical representation of the D_{CT}).

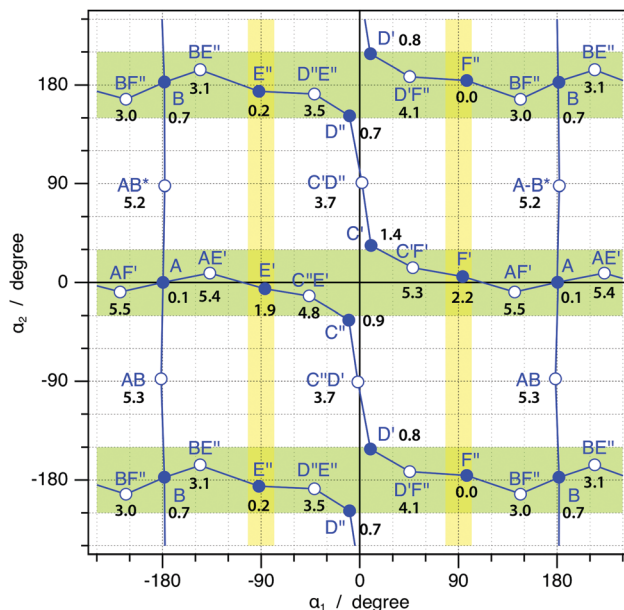


Fig. 7 Bi-dimensional PES of GLAC^{-1} in its lowest excited state (*i.e.*, S_1). The numbers indicated are the $\Delta\Delta G$ energies in kcal mol^{-1} relative to the more stable minimum **F''**. Filled circles are minima and empty circles are transition states. Blue lines indicate the real connections between conformers. We have also highlighted with a green band the zones where α_2 is almost 0° or $\pm 180^\circ$. In all ES minima, the NH bridge is close to coplanar with the acridone moiety. Yellow bands indicate the region of the non-emitting species. Notation: **A** corresponds to the minimum **ES-A** and **AE'** to the **TS ES-AE'**.

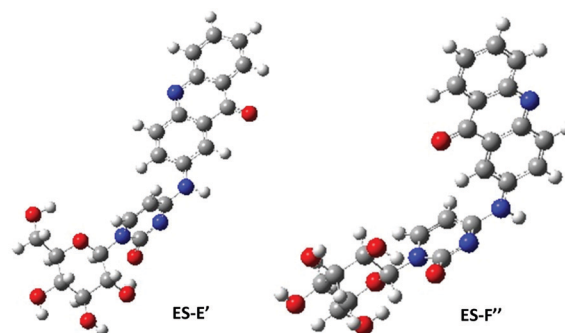


Fig. 8 Fully-optimized minimum-energy geometries of the **ES-E'** and **ES-F''** conformers on the S_1 excited-state PES. In both these conformers, the acridone and the cytosine are mutually orthogonal, leading to the formation of a TICT state.

As observed, the D_{CT} indexes of the non-emitting species show a spatial charge separation significantly higher than for the other minima, indicating the above-mentioned charge-shift.

All the S_1 conformers have similar energies and their difference is not higher than $2.2 \text{ kcal mol}^{-1}$, with the twisted conformer **ES-F''** being the most stable one (see Table S3, ESI†). In comparison with the ground state PES, the rotational barriers around α_1 decrease and those around α_2 increase slightly. Moreover, both the average distances of the ${}^4\text{N}-{}^2\text{C}$ and ${}^4\text{N}-{}^4\text{C}$ bonds are 1.38 \AA , for all S_1 conformers. This indicates that, in the excited state, both the ${}^4\text{N}-{}^2\text{C}$ and ${}^4\text{N}-{}^4\text{C}$ bonds are even longer than the

typical partial double amidic bond (*i.e.*, approx. 1.32 Å), suggesting that free rotation around both α_1 and α_2 is allowed and that the formation of stable twisted minima becomes favoured (see Table S2, ESI†).

4.3 Spectroscopic properties

Electronic absorption. For each of the seven ground-state conformers, we calculated, through TD-DFT methods, the six lowest-energy electronic transitions. For the sake of clarity, only the properties of the $S_0 \rightarrow S_1$ electronic transition are reported in Table 3 for all conformers.

For all the ground-state conformers, the $S_0 \rightarrow S_1$ electronic transition can be described as an almost pure HOMO \rightarrow LUMO excitation. Since the HOMO is mainly localized on the acridone and the LUMO is delocalized over both the acridone and the cytosine moieties (Fig. 9), the $S_0 \rightarrow S_1$ transition has a mixed character. On the one hand, there is a π - π^* local-excited (LE) contribution from the acridone π system; on the other hand, a charge-transfer (CT) component implies the excitation of one electron from the acridone to the cytosine moiety.

For values of the dihedral angle α_2 far from zero, like for conformers **GS-D'** and **GS-D''** ($\alpha_2 = 128.0^\circ$ and 127.5° , Table 3) the LE character prevails since both π - π^* orbitals are localized on the acridone.

The $S_0 \rightarrow S_1$ transition energy, computed at the M062X level, is approx. 75.4 kcal mol⁻¹ for all conformers in water and only a minor red shift is observed in the case of the planar conformer

Table 3 Relevant structural and spectroscopic parameters computed for all GLAC⁻¹ ground-state conformers: dihedral angles α_1 and α_2 ; Boltzmann population of the different ground-state conformers at 300 K; energy (E) and oscillator strength (f) corresponding to the $S_0 \rightarrow S_1$ electronic transition; and population in the Franck–Condon state, determined as $p_{FC} = 100 \cdot p_{GS} \cdot f_i / \sum p_{GS} \cdot f_i$

Isomer	Angle α_1	Angle α_2	p_{GS} (%)	E (kcal mol ⁻¹)	f	p_{FC} (%)
GS-A'	+173.9	-32.1	6.0	75.4	0.162	8
GS-A''	-173.2	+32.1	9.9	75.3	0.164	13
GS-B	-179.1	+176.7	2.5	74.0	0.085	2
GS-C'	+4.2	+56.2	31.5	75.7	0.133	33
GS-C''	-3.8	-57.4	22.3	75.7	0.131	23
GS-D'	+4.5	-128.0	16.3	75.5	0.099	13
GS-D''	-4.3	+127.5	11.5	75.5	0.100	9

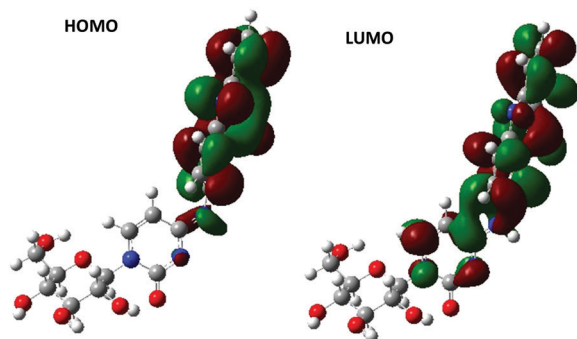


Fig. 9 HOMO and LUMO orbitals, corresponding to the lowest transition of the most stable conformer **GS-C'**.

Table 4 Emission properties computed at the M062X level for the GLAC⁻¹ conformers in water (using PCM); emission energy (E), oscillator strength (f) and Stokes shift (kcal mol⁻¹)

Conformer	E (kcal mol ⁻¹)	f	Stokes shift
ES-A	67.4	0.153	7.9
ES-B	69.3	0.088	4.7
ES-C'	69.0	0.114	6.7
ES-C''	69.1	0.118	6.6
ES-D'	68.9	0.087	6.6
ES-D''	68.8	0.096	6.7
ES-E'	5.6	0.000	
ES-E''	9.1	0.001	
ES-F'	9.2	0.001	
ES-F''	8.7	0.001	

GS-B (*i.e.*, 74.0 kcal mol⁻¹, see Table 3). This conformer is characterised by $f = 0.085$, the lowest oscillator strength; f increases for the other mirrored couples of conformers, following the trend **GS-A** > **GS-C** > **GS-D**.

Emission. Apart from the two **ES-E** and **ES-F** couples, the relaxation from the Franck–Condon region to the excited state minimum involves a charge shift from acridone to cytosine. The two linear **GS-A** conformers emit from the same **ES-A** planar conformer, at 65.7 kcal mol⁻¹ with an oscillator strength of 0.199 (Table 4).

It is certain, although in a qualitative manner, that the transformation of the two ground state minima in the excited state surface is coupled with the second vibrational mode α_2 of the two **GS-A** minima (*e.g.*, 15.85 cm⁻¹ for **GS-A'**). This normal mode is due to the opposite rotation of the two aromatic groups around the NH bridge. **GS-B** remains planar in the excited state and the normal vibrational mode corresponding to the rotation between the two aromatic groups is the first at 14.01 cm⁻¹.

This behaviour is similar in the two couples **GS-C** and **GS-D**, where this transformation is coupled with the first vibrational mode (*e.g.*, ν_1 at 10.46 cm⁻¹ for **GS-C''** and ν_1 at 14.83 cm⁻¹ for **GS-D'**, respectively, see Fig. 10) and is due to rotation around the α_2 angle.

The steric hindrance between the hydrogens of the acridone moiety (C-1'' or C-3'') and the hydrogen of the NH bridge, on the one hand hinders planarisation of the structure, and on the other favours transition toward the non-emitting couples of minima **ES-E** and **ES-F** (emission at around 6–9 kcal mol⁻¹ with an oscillator strength of 0.00). The two aromatic planes rotate in opposite directions becoming orthogonal. The orthogonality of the two planes results in a lack of overlap between the

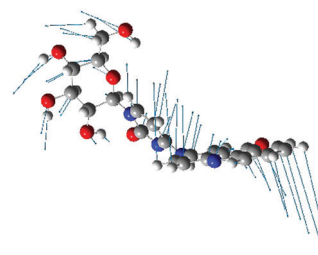


Fig. 10 Lower vibrational mode computed for the **GS-C''** minimum.

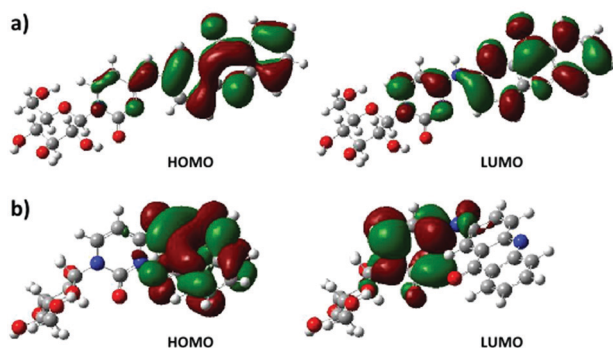


Fig. 11 HOMO and LUMO orbitals: (a) in the planar excited-state conformer **ES-A**, the orbitals are delocalized over the two aromatic rings. (b) In the twisted non-emissive conformer **ES-F**, the HOMO is localized on the acridone while the LUMO is on the cytosine moiety.

HOMO and LUMO, corresponding to a charge transfer transition from acridone to the cytosine moiety. The difference between the orbitals of one emitting species (**ES-D'**) and one non-emitting species (**ES-F''**) is illustrated in Fig. 11. The excited state surface shows the existence of non-emitting species next to various emitting conformational minima. The nature of the dark states, evaluated using the SS (State-Specific) model, suggests the presence of conical intersections close to the S_1 minima. In fact, the evaluated emission energies are about 7 ± 2 kcal mol⁻¹, which are in the IR region where a conical intersection can be reached, thanks to vibrational coupling between S_0 and S_1 .

In general, TD-DFT methods cannot provide an accurate description of the conical intersections and the investigation of the deactivation dynamics, possibly requiring wave-function multi-configurational methods, is out of the scope of the present work.

The excited state description of the S_1 surface has been validated using a long-range density functional like CAM-B3LYP.³² The studied systems, **ES-A**, **TS ES-AF'** and **ES-F'**, show the same characteristics (geometries, orbitals and transition energies) as those derived using the M062X functional (see Table 4 and Fig. S4, ESI†).

In Fig. 12 are gathered both the ground-state and the lowest excited-state potential energy surfaces of GLAC⁻¹, reported as a function of both α_1 and α_2 dihedral angles. This overlap between the S_0 and S_1 PESs allows an easier evaluation of all the possible deactivation pathways that the system may follow right after vertical excitation from S_0 minima to S_1 .

As an example, the position of **GS-D'** in the ground state corresponds to its Frank–Condon position after absorption and makes it possible to see which minima of the excited state can be reached easily. In this case, the more easily accessible minimum is **ES-D'** which can evolve to **ES-C''** or to the most stable minimum of the S_1 surface, the non-emitting species **ES-F''**, through an energy barrier of 3.3 kcal mol⁻¹.

The PESs of the ground and excited states provide a detailed picture of the photophysical behaviour of the GLAC⁻¹ in water. The flat PES of the excited state, where emitting and non-emitting species are directly connected, is due to a reorganisation involving mutual rotation around the two dihedral angles α_1 and α_2 which provokes, alternatively, localisation and delocalisation of the π HOMO and LUMO orbitals involved in the excitation.

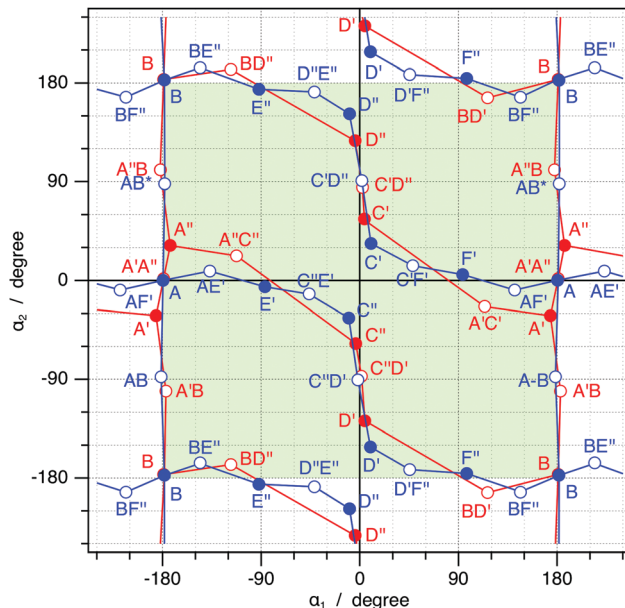


Fig. 12 PES of the ground state S_0 and of the first excited state S_1 determined for the various conformers of GLAC⁻¹. Filled circles are minima and empty circles are transition states with the corresponding lines describing the real connections between them (red: ground state; blue: excited state). The picture is an overlap of Fig. 6 and 7.

Table 5 Fluorescence anisotropies computed at the DFT M062X level for various combinations of absorbing and emitting conformers of GLAC⁻¹

	A_{abs}	B_{abs}	C_{abs}	D_{abs}
A_{emi}	0.21	0.12	-0.19	-0.15
B_{emi}	-0.02	0.40	-0.16	-0.18
C_{emi}	-0.19	-0.16	0.35	-0.19
D_{emi}	-0.19	0.11	-0.18	0.17
E_{emi}	-0.16	-0.20	0.20	-0.20
F_{emi}	-0.12	-0.11	0.07	0.23

This structural rearrangement corresponds to a decrease of the ⁴N–⁴C bond order coinciding with an increase of the ⁴N–²C bond order. In the ground state, rotation around α_1 has a quite large barrier which inhibits mixing between *Z* and *E* isomers. In the S_1 surface these barriers are lower by at least one third and in principle could permit the photoinduced isomerization of the molecule. Moreover, the analysis of the excited state orbitals shows that rotation around the two aromatic planes defined by the acridone and cytosine moieties, leads to the formation of dark states; this is due to non-overlapping HOMO–LUMO orbitals and happens when the dihedral angle α_2 is close to 90° (Fig. 9).

Finally, the fluorescence anisotropy was calculated using the formula $r_0 = 2((3 \cos^2 \beta - 1)/2)/5$, where β is the angle between the absorption and emission dipoles (Table 5).

5 Discussion

The experimental part of our work showed that GLAC⁻¹ in neutral aqueous solution emits fluorescence with a quantum

yield of 0.09. This is about ten times lower than that of acridone (*ca.* 1)³³ but much higher than that of cytosine (*ca.* 10⁻⁴),³⁴ suggesting the existence of important electronic interactions between the two aromatic moieties of the compound. Our computational part rationalised these interactions and revealed a very rich conformational landscape, both in the ground state and in the first excited state. The properties of the computed potential energy surfaces will help us to explain the complex behaviour observed by our time-resolved measurements.

Our calculations identified four classes of stable conformers (*i.e.*, a planar conformer and three couples of mirrored ones) that we called **GS-A**, **GS-B**, **GS-C** and **GS-D**, differing in the way that the two aromatic moieties are rotated with respect to each other (Fig. 5). The ground state populations at room temperature, p_{GS} , were found to be 15.9, 2.5, 53.8 and 27.8%, respectively, for **GS-A**, **GS-B**, **GS-C** and **GS-D**. Isomerisation is governed by two independent rotations around the angles α_1 and α_2 and may lead to the formation of non-emitting TICT states, for which the two planar groups are mutually orthogonal. We identified two couples of twisted intramolecular charge transfer (TICT) states (**ES-E** and **ES-F**) increasing the number of excited state minima from 7 to 10; **A'** and **A''** conformers evolved towards the same minimum.

Although TICT formation has been largely studied,^{35–40} the concerted rotation around two dihedral angles has been less explored. Recently, G. Haberhauer⁴¹ has studied fluorophores where donor and acceptor groups have a predetermined sequence and has used, similar to our work, two independent rotations, originating from the presence of π -conjugated, NH linked moieties, to combine TICT and PLICT⁴² (or PICT, planarised intramolecular charge transfer states).¹⁸

In our case, the charge transfer is possible because, upon rotation around angle α_1 , the π orbitals of acridone conjugated with the lone-pair of the nitrogen bridge give rise to a good electron donating group compared to a good cytosine acceptor. Simple rotation around α_2 , where the NH bridge remains within the cytosine plane, does not allow the formation of a TICT state and only transition states are detected. For a given α_1 , rotation around the α_2 dihedral leads to the most favourable disposition of the two aromatic groups.

Coming to the spectroscopic aspects, our computations show that for all conformers, the first Franck–Condon excited state S_1 is well-separated in energy from the second state by at least 12 kcal mol⁻¹. Moreover, the $S_0 \rightarrow S_1$ transition energy is quite similar for all conformers (Table 3), their difference not exceeding 1.6 kcal mol⁻¹. Therefore, the absorption band in Fig. 2 is in fact an envelope of the transitions associated with the four conformers. A closer comparison between the experimental absorption spectrum (Fig. 2) and the computed transition energies (Table 3) shows that the latter are overestimated. This inaccuracy is due to the fact that (i) the functional M062X, used in our computations, overestimates the electronic transition energies but without a drift⁴³ between the locally excited and charge transfer transitions and (ii) vibrational/thermal effects are not taken into account. The contribution of each one conformer i to the Franck–Condon

excited state p_{FC} is given as $p_{GSi} \times f_i / \sum(p_{GSi} \times f_i)$, where f is the oscillator strength (Table 3). The average computed oscillator strength $\langle f \rangle = \sum(p_{GSi} \times f_i) / 100$ is 0.12, a value in line with the maximum molar extinction coefficient of 5300 mol⁻¹ L cm⁻¹ determined experimentally (Fig. 2). Moreover, the computed Stokes shifts are 5–8 kcal mol⁻¹, not very different from the experimental values, 7 and 11 kcal mol⁻¹, determined by either considering the shoulder or the peak of the fluorescence spectrum (Fig. 2).

From steady-state and time-resolved experiments, we deduce that the emission spectrum is correlated mainly with a time constant of 7.9 ns. A second time-constant of 0.5 ns, whose amplitude is larger at shorter wavelengths, contributes by less than 4% to the emitted photons (Table 1). It could be correlated with the high energy shoulder (Fig. 2a), as suggested from experiments performed with GLAC in acetonitrile (Fig. 2b and Table 1). Moreover, from the anisotropy values recorded on the 100 ps scale (Fig. 4), it appears that the emitting species with a lifetime of 0.5 ns is characterised by higher anisotropy. Given these considerations on the polarisation of the electronic transitions associated with the fluorescent species, we propose, at a first approach, a possible correlation between experimental and computed results. Thus, **ES-A** and **ES-D**, characterised by a fluorescence anisotropy of 0.21 and 0.17, respectively (Table 5), are candidates for the 7.9 ns constant. Conversely, **ES-B** and **ES-C** for which the computed anisotropies are higher (0.40 and 0.35, respectively) are candidates for the 0.5 ns time constant. One could think that, by some coincidence, the fluorescence dynamics are identical for the emitting minima of each pair. Yet, in view of the difference in the oscillator strength values calculated for each pair (Table 4: 0.20 and 0.10 for the first one, 0.11 and 0.15 for the second), together with the precision of our TCSPC measurements (error in the time constants: 0.1 ns), such a scenario does not seem plausible. This is particularly true for the largest time constant.

The quenching of the fluorescence stemming from a given conformer **X** depends on its propensity to undergo **X** \rightarrow **Y** isomerization toward another conformer **Y**, emitting or not, which is determined by the energy barrier ΔE_{XY} . These values, calculated considering as zero the excited state minimum **ES-X**, are shown in Table 6.

We also report the excess of energy, in respect to this barrier, resulting from the Franck–Condon transition, ΔE_{FC} . Although the loss of excess energy (vibrational relaxation, thermalisation) is expected to be much faster than the isomerisation process, we cannot rule out that, to some extent, it may favour overcoming the barrier. Finally, in Table 6 we report the half-life $t_{1/2}$ of **X**, in respect to the transformation **X** \rightarrow **Y**, determined *via* the Eyring equation⁴⁴ as follows:

$$k = \kappa \cdot (k_B T / h) \cdot \exp(-\Delta E / RT) \quad \text{and} \quad t_{1/2} = \ln(2) / k$$

where, k_B , h and R are, respectively, the Boltzmann, Planck and gas constants and T is the absolute temperature; the transmission coefficient κ was set to 1. The values are not expected to correspond to the experimentally determined lifetimes, but simply indicate differences in the dynamical behaviour of the various conformers.

Table 6 Single step energy barriers that may affect transformation of isomer **X** to isomer **Y** (and *vice versa*) in the first excited state of GLAC⁻¹. $\Delta\Delta G$: energy barriers with respect to the **X** and **Y** minimum. $t_{1/2}$: half times of **X** and **Y** determined via the Eyring equation. ΔE_{FC} : excess of energy with respect to the barrier, resulting from the Franck–Condon excitation of **X** and **Y** calculated as: $\Delta E_{FC} = (\Delta\Delta G_{\text{ground state}} + \text{energy transition} - \Delta\Delta G_{\text{excited state}})$. All calculations were carried out at the 6-311g** basis set level

XY	$\Delta\Delta G^a$	$\Delta\Delta G^a$	$t_{1/2}^b$	$t_{1/2}^b$	ΔE_{FC}^a	ΔE_{FC}^a
	X → Y	X ← Y	X → Y	X ← Y	X → Y	X ← Y
AB	5.2	4.6	681	210	5.3	9.3
AB*	5.1	4.5	576	210	5.3	9.3
AE'	5.3	3.5	805	39	5.2	—
AF'	5.4	3.3	952	28	5.1	—
BE''	2.4	2.9	6	14	6.4	—
BF''	2.3	3	5	17	6.5	—
C'D''	2.3	3	5	17	6.3	6.8
C'F'	3.9	3.1	77	20	4.6	—
C''D'	2.8	2.9	12	14	6.5	6.6
C''E'	3.9	2.9	77	14	5.7	—
D'F''	3.3	4.1	28	108	6.2	—
D''E''	2.8	3.3	12	28	7.0	—

^a In kcal mol⁻¹. ^b In ps.

From Table 6, we could remark on two extreme cases. On the one side, the highest energy barriers, the lowest excess energy ΔE_{FC} and the longest $t_{1/2}$ values are encountered for conformer **A**. Therefore, we deduce that this conformer is responsible for the fluorescence component characterised by a lifetime of 7.9 ns. On the other side, conformer **B** is characterised by the lowest energy barriers and the highest excess energy, making its evolution toward TICT states highly probable. Such dynamical factors, associated with the fact that the contribution of **B** to the Franck–Condon population is only 2%, preclude detection of fluorescence arising from **B**. Therefore, we assign the 0.5 ns fluorescence lifetime to **C** conformers, characterised by intermediate $t_{1/2}$ values and energy barriers, their evolution toward TICT states (**ES-E** and **ES-F**) being only partial. TICT states are known to be stabilised in polar solvents.⁴⁵ Accordingly, one could assign to this effect the observed decrease of fluorescence quantum yield of GLAC in water compared to acetonitrile (0.09 vs. 0.22). Moreover, as the energy barriers leading to TICT are lower for **ES-C** than for **ES-A** conformers, the fluorescence lifetime of the former undergoes more important decrease (from 1.3 to 0.5 ns) than that of the latter (from 9.6 to 7.9 ns). However, in the present case, such an interpretation is oversimplified because GLAC in neutral aqueous solution is present as a monoanion. An additional interpretation could be based on the behaviour of the ground state. In the case of the non-emitting **ES-E** and **ES-F** conformers, the energy gap between S_0 and S_1 is very low, possibly arising from higher destabilisation of the corresponding ground-state twisted structures, due to the non-equilibrium solvation. We expect that this destabilization is higher in aqueous buffer than in acetonitrile.

Finally, regarding our experimental observations on the ps time-scale, we stress that the fluorescence upconversion technique is capable of probing photons associated with quantum yields as low as 10^{-6} .⁴⁶ In other words, it can detect emitting species whose fingerprint is not present in the steady-state

fluorescence spectra. In a qualitative way, we attribute the important decay at 430 nm observed for GLAC⁻¹ aqueous solutions to transformations of the **C** conformers and the weak rise at 515 nm to the appearance of the **D** conformer, which subsequently evolves toward TICT states. We already mentioned **C** as a candidate for the 0.5 ns time constant. However, as the values reported in Table 6 for the mirror images **C'** and **C''** are somewhat different, it is possible that their dynamics are also different. Alternatively, the decays at short time-scales could have a non-exponential behaviour and our fits provide only a phenomenological picture. A temperature dependent study of the ultrafast decay and rise should certainly bring valuable information about these processes. But such measurements are very delicate on this time-scale and our setup is not equipped to this end. In addition, at this time-scale, we also have contribution from the solvent relaxation. We assign to this process the 1 ps time-constant, which is typical for aqueous solutions.^{47,48}

6 Conclusion and outcome

We have presented a study on the fluorescence of GLAC, a recently described potent inhibitor of glycogen phosphorylase. The most important part of our work dealt with free GLAC in aqueous neutral solution, where it exists in its mono-anionic form. Combination of multiscale time-resolved spectroscopy with quantum chemistry calculations revealed a quite complex behaviour in the excited state relaxation.

Our calculations evidenced the existence of four classes of conformers in the ground state of GLAC⁻¹, resulting from mutual rotation of the acridone and cytosine components around two dihedral angles. The number of conformers further increases in the first electronically excited state where the formation of twisted intermolecular charge transfer states results in partial quenching of the fluorescence. The fingerprints of several conformers were detected experimentally in the fluorescence dynamics; they were identified using the polarisation of their electronic transitions as criterium. Despite this diversity, the steady-state fluorescence spectrum, characterised by a quantum yield of 0.09, arises from a single conformer whose lifetime is 7.9 ns.

GLAC is the first fluorescent inhibitor of glycogen phosphorylase. In neutral aqueous solutions, its fluorescence peaks around 465 ± 10 nm, both in its free form and when bound to the enzyme. Though its fluorescence decreases upon binding, it is still possible to properly study its dynamic behaviour.⁴⁹ The observation that, on the one hand, GLAC appears to adopt a bisanionic form within its complex with GP⁴ and, on the other, free GLAC⁻² in solution is not emitting (Fig. 3), suggests the existence of a subtle interplay between rotation and deprotonation processes. In order to fully assess these processes, computations taking into account the detailed local environment within the enzyme pocket are currently in progress. The identification of the factors responsible for the partial quenching of GLAC fluorescence will allow the design of novel fluorescent 1-aryl- β -D-glucopyranose derivatives.

Beyond the importance of the present study related to the potential therapeutic action of 1-aryl- β -D-glucopyranose derivatives

and their use as labels for probing dynamical interactions with glycogen phosphorylase, our computational work may be viewed as a more general showcase. As a matter of fact, although numerous computational studies describe excited state surfaces involving mutual rotation between two aromatic moieties, here we show how two independent rotations may rule the process in a subtle equilibrium, potentially leading to the formation of a TICT state. Rotation of the dihedral angle α_2 is responsible for charge transfer which is possible only if the nitrogen lone pair of the bridge is part of the π orbitals of the acridone moiety. In other words, only in this case, the acridone moiety behaves as a donor with respect to the cytosine moiety that acts like an acceptor. Rotation around α_2 simply assists α_1 for finding the most favourable disposition of the two aromatic groups. Simple rotation around α_2 , where the NH bridge remains planar with cytosine, does not allow the formation of a TICT state and transition states are detected.

Conflicts of interest

There are no conflicts to declare.

Acknowledgements

This work was supported by Heracleitus II (awarded to M. M), LASERLAB-EUROPE (FP7 No. 284464) and “Progetto Bandiera” N-CHEM (to A. V). K. M. acknowledges funding from the Hellenic National Scholarships Foundation through a “Strengthening of Human Resources through Doctoral Research” program, co-financed by the European Union (European Social Fund ESF) and Greek national funds through the Operational Program “Human Resource Development, Education and Lifelong Learning” 2014–2020.

References

- 1 E. D. Chrysina, *Mini-Rev. Med. Chem.*, 2010, **10**, 1093–1101.
- 2 T. Gimisis, *Mini-Rev. Med. Chem.*, 2010, **10**, 1127–1138.
- 3 L. Agius, *Mol. Aspects Med.*, 2015, **46**, 34–45.
- 4 M. Mamais, A. Degli Esposti, V. Kouloumoundra, T. Gustavsson, F. Monti, A. Venturini, E. D. Chrysina, D. Markovitsi and T. Gimisis, *Chem. – Eur. J.*, 2017, **23**, 8800–8805.
- 5 T. Hadjiloi, C. Tiraidis, E. D. Chrysina, D. D. Leonidas, N. G. Oikonomakos, P. Tsipos and T. Gimisis, *Bioorg. Med. Chem.*, 2006, **14**, 3872–3882.
- 6 C. Tiraidis, K.-M. M. Alexacou, S. E. Zographos, D. D. Leonidas, T. Gimisis and N. G. Oikonomakos, *Protein Sci.*, 2007, **16**, 1773–1782.
- 7 Y. Liu, C. H. Wolstenholme, G. C. Carter, H. Liu, H. Hu, L. S. Grainger, K. Miao, M. Fares, C. A. Hoelzel, H. P. Yennawar, G. Ning, M. Du, L. Bai, X. Li and X. Zhang, *J. Am. Chem. Soc.*, 2018, 8–11.
- 8 O. Tietz, J. Kaur, A. Bhardwaj and F. R. Wuest, *Org. Biomol. Chem.*, 2016, **14**, 7250–7257.
- 9 G. Leriche, A. C. Chen, S. Kim, D. J. Selkoe and J. Yang, *ACS Chem. Neurosci.*, 2016, **7**, 40–45.
- 10 L. C. Kenmogne, R. Maltais and D. Poirier, *Bioorg. Med. Chem. Lett.*, 2016, **26**, 2179–2183.
- 11 A. Thorarensen, R. W. Sarver, F. Tian, A. Ho, D. L. Romero and K. R. Marotti, *Bioorg. Med. Chem. Lett.*, 2007, **17**, 4646–4649.
- 12 M. Kondo, I. A. Heisler and S. R. Meech, *J. Phys. Chem. B*, 2010, **114**, 12859–12865.
- 13 L. Dehmel, F. Berndt, M. Weinberger, M. Sajadi, I. Ioffe, H.-A. Wagenknecht and N. P. Ernsting, *Phys. Chem. Chem. Phys.*, 2016, **18**, 6813–6820.
- 14 J. S. Beckwith, A. Rosspeintner, G. Licari, M. Lunzer, B. Holzer, J. Fröhlich and E. Vauthey, *J. Phys. Chem. Lett.*, 2017, **8**, 5878–5883.
- 15 D. Zhong, S. K. Pal, C. Wan and A. H. Zewail, *Proc. Natl. Acad. Sci. U. S. A.*, 2001, **98**, 11873–11878.
- 16 C. Martín, M. Gil, B. Cohen and A. Douhal, *Langmuir*, 2012, **28**, 6746–6759.
- 17 I. Vayá, P. Bonancía, M. C. Jiménez, D. Markovitsi, T. Gustavsson and M. A. Miranda, *Phys. Chem. Chem. Phys.*, 2013, **15**, 4727.
- 18 P. H. Gore and G. K. Hughes, *J. Chem. Soc.*, 1959, 1615–1616.
- 19 M. M. Barnett, A. H. C. P. Gillieson and W. O. Kermack, *J. Chem. Soc.*, 1934, 433–435.
- 20 M. Mamais, V. Kouloumoundra, E. Smyrli, P. Grammatopoulos, E. D. Chrysina and T. Gimisis, *Tetrahedron Lett.*, 2015, **56**, 5549–5552.
- 21 T. Gustavsson, L. Cassara, V. Gulbinas, G. Gurzadyan, J.-C. Mialocq, S. Pommeret, M. Sorgius and P. van der Meulen, *J. Phys. Chem. A*, 1998, **102**, 4229–4245.
- 22 M. Caricato, B. Mennucci, J. Tomasi, F. Ingrosso, R. Cammi, S. Corni and G. Scalmani, *J. Chem. Phys.*, 2006, **124**, 94107.
- 23 J. Tomasi, B. Mennucci and R. Cammi, *Chem. Rev.*, 2005, **105**, 2999–3093.
- 24 M. J. Frisch, G. W. Trucks, H. B. Schlegel, G. E. Scuseria, M. A. Robb, J. R. Cheeseman, G. Scalmani, V. Barone, G. A. Petersson, H. Nakatsuji, X. Li, M. Caricato, A. V. Marenich, J. Bloino, B. G. Janesko, R. Gomperts, B. Mennucci, H. P. Hratchian, J. V. Ortiz, A. F. Izmaylov, J. L. Sonnenberg, D. Williams-Young, F. Ding, F. Lipparini, F. Egidi, J. Goings, B. Peng, A. Petrone, T. Henderson, D. Ranasinghe, V. G. Zakrzewski, J. Gao, N. Rega, G. Zheng, W. Liang, M. Hada, M. Ehara, K. Toyota, R. Fukuda, J. Hasegawa, M. Ishida, T. Nakajima, Y. Honda, O. Kitao, H. Nakai, T. Vreven, K. Throssell, J. A. Montgomery Jr., J. E. Peralta, F. Ogliaro, M. J. Bearpark, J. J. Heyd, E. N. Brothers, K. N. Kudin, V. N. Staroverov, T. A. Keith, R. Kobayashi, J. Normand, K. Raghavachari, A. P. Rendell, J. C. Burant, S. S. Iyengar, J. Tomasi, M. Cossi, J. M. Millam, M. Klene, C. Adamo, R. Cammi, J. W. Ochterski, R. L. Martin, K. Morokuma, O. Farkas, J. B. Foresman and D. J. Fox, *Gaussian 16, Revision B.01*, Gaussian Inc., Wallingford CT, 2016.
- 25 Y. Zhao and D. G. Truhlar, *Acc. Chem. Res.*, 2008, **41**, 157–167.
- 26 R. Improta, *Phys. Chem. Chem. Phys.*, 2008, **10**, 2656–2664.
- 27 F. Santoro, V. Barone and R. Improta, *J. Am. Chem. Soc.*, 2009, **131**, 15232–15245.

- 28 R. Improta, G. Scalmani, M. J. Frisch and V. Barone, *J. Chem. Phys.*, 2007, **127**, 74504.
- 29 R. Improta, V. Barone, G. Scalmani and M. J. Frisch, *J. Chem. Phys.*, 2006, **125**, 54103.
- 30 C. Adamo, T. Le Bahers, M. Savarese, L. Wilbraham, G. García, R. Fukuda, M. Ehara, N. Rega and I. Ciofini, *Coord. Chem. Rev.*, 2015, **304–305**, 166–178.
- 31 A. M. Brouwer, *Pure Appl. Chem.*, 2011, **83**, 2213–2228.
- 32 T. Yanai, D. P. Tew and N. C. Handy, *Chem. Phys. Lett.*, 2004, **393**, 51–57.
- 33 M. Siegmund and J. Bendig, *Z. Naturforsch., A: Phys. Sci.*, 1980, **35**, 1076–1086.
- 34 L. Martínez-Fernández, A. J. Pepino, J. Segarra-Martí, J. Jovaišaitė, I. Vaya, A. Nenov, D. Markovitsi, T. Gustavsson, A. Banyasz, M. Garavelli and R. Improta, *J. Am. Chem. Soc.*, 2017, **139**, 7780–7791.
- 35 D. Su, C. L. Teoh, L. Wang, X. Liu and Y.-T. Chang, *Chem. Soc. Rev.*, 2017, **46**, 4833–4844.
- 36 F. Monti, A. Venturini, A. Nenov, F. Tancini, A. D. Finke, F. Diederich and N. Armaroli, *J. Phys. Chem. A*, 2015, **119**, 10677–10683.
- 37 *Conformational Analysis of Molecules in Excited States*, ed. J. Waluk, Wiley-VCH, 2000.
- 38 Z. R. Grabowski, K. Rotkiewicz and W. Rettig, *Chem. Rev.*, 2003, **103**, 3899–4031.
- 39 P. B. Coto, L. Serrano-Andrés, T. Gustavsson, T. Fujiwara and E. C. Lim, *Phys. Chem. Chem. Phys.*, 2011, **13**, 15182–15188.
- 40 D. Markovitsi, H. Sigal, C. Ecoffet, P. Millié, F. Charra, C. Fiorini, J.-M. Nunzi, H. Strzelecka, M. Veber and C. Jallabert, *Chem. Phys.*, 1994, **182**, 69–80.
- 41 G. Haberhauer, *Chem. – Eur. J.*, 2017, **23**, 9288–9296.
- 42 G. Haberhauer, R. Gleiter and C. Burkhardt, *Chem. – Eur. J.*, 2016, **22**, 971–978.
- 43 C. Adamo and D. Jacquemin, *Chem. Soc. Rev.*, 2013, **42**, 845–856.
- 44 H. Eyring, *Chem. Rev.*, 1935, **17**, 65–77.
- 45 Z. R. Grabowski, K. Rotkiewicz and W. Rettig, *Chem. Rev.*, 2003, **103**, 3899–4032.
- 46 P. Changenet-Barret, T. Gustavsson, D. Markovitsi and I. Manet, *ChemPhysChem*, 2016, **17**, 1264–1272.
- 47 R. Jimenez, G. R. Fleming, P. V. Kumar and M. Maroncelli, *Nature*, 1994, **369**, 471–473.
- 48 W. Jarzeba, G. C. Walker, A. E. Johnson, M. A. Kahlow and P. F. Barbara, *J. Phys. Chem.*, 1988, **92**, 7039–7041.
- 49 E. D. Chrysina, T. Gimisis, T. Gustavsson, M. Mamais and D. Markovitsi, Unpubl. results.